

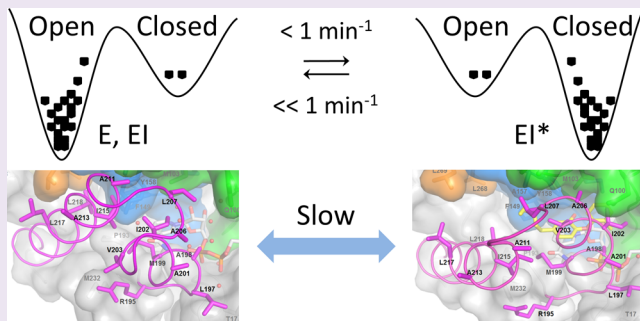
A Structural and Energetic Model for the Slow-Onset Inhibition of the *Mycobacterium tuberculosis* Enoyl-ACP Reductase InhA

Huei-Jiun Li,^{§,#} Cheng-Tsung Lai,^{‡,||,#} Pan Pan,[§] Weixuan Yu,[§] Nina Liu,[§] Gopal R. Bommneni,[§] Miguel Garcia-Diaz,[†] Carlos Simmerling,^{*,†,||,‡,§} and Peter J. Tonge^{*,†,||,§}

[†]Institute for Chemical Biology and Drug Discovery, [‡]Laufer Center for Physical and Quantitative Biology and [§]Department of Chemistry, ^{||}Graduate Program in Biochemistry and Structural Biology, and [¶]Department of Pharmacological Sciences, Stony Brook University, Stony Brook, New York 11794, United States

Supporting Information

ABSTRACT: Slow-onset enzyme inhibitors are of great interest for drug discovery programs since the slow dissociation of the inhibitor from the drug–target complex results in sustained target occupancy leading to improved pharmacodynamics. However, the structural basis for slow-onset inhibition is often not fully understood, hindering the development of structure-kinetic relationships and the rational optimization of drug-target residence time. Previously we demonstrated that slow-onset inhibition of the *Mycobacterium tuberculosis* enoyl-ACP reductase InhA correlated with motions of a substrate-binding loop (SBL) near the active site. In the present work, X-ray crystallography and molecular dynamics simulations have been used to map the structural and energetic changes of the SBL that occur upon enzyme inhibition. Helix-6 within the SBL adopts an open conformation when the inhibitor structure or binding kinetics is substrate-like. In contrast, slow-onset inhibition results in large-scale local refolding in which helix-6 adopts a closed conformation not normally populated during substrate turnover. The open and closed conformations of helix-6 are hypothesized to represent the EI and EI* states on the two-step induced-fit reaction coordinate for enzyme inhibition. These two states were used as the end points for nudged elastic band molecular dynamics simulations resulting in two-dimensional potential energy profiles that reveal the barrier between EI and EI*, thus rationalizing the binding kinetics observed with different inhibitors. Our findings indicate that the structural basis for slow-onset kinetics can be understood once the structures of both EI and EI* have been identified, thus providing a starting point for the rational control of enzyme–inhibitor binding kinetics.



Slow-onset enzyme inhibitors are compounds in which formation of the enzyme–inhibitor complex occurs on the time scale of standard enzyme assays.^{1,2} Such compounds are of particular interest in drug discovery programs since the rate of complex dissociation (k_{off}) can be slower than the time scale of *in vivo* drug metabolism and elimination, leading to sustained target occupancy and improved *in vivo* efficacy.^{3–6} In order to modulate drug action, it follows that a detailed mechanistic understanding is required of the molecular factors that control the rate of enzyme–inhibitor complex formation and breakdown,⁷ which in the current context is slow relative to many of the common motions associated with biological macromolecules (Figure 1).

In an effort to develop novel antibacterial agents, we have developed inhibitors of the NAD(P)H-dependent FabI enoyl-ACP reductase from the bacterial fatty acid biosynthesis (FASII) pathway (Figure 2).^{4,7–13} In the course of this work we identified a series of diphenyl ethers that are slow-onset inhibitors of the FabI enzyme from *Francisella tularensis* and in which a correlation was observed between the lifetime of the enzyme–inhibitor complex and *in vivo* efficacy, supporting the

importance of drug-target residence time ($1/k_{\text{off}}$) as a key parameter in lead optimization.⁴ This prompted us to identify time-dependent inhibitors of the FabI enzymes from other organisms including that from the important human pathogen *Mycobacterium tuberculosis* (InhA) and to explore the mechanistic basis for slow-onset inhibition.^{8,14} The diphenyl ether inhibitors of InhA bind uncompetitively and form a ternary complex with the InhA:NAD⁺ product complex. Time-dependent inhibition is observed for the potent inhibitor PT70 (Table 1), where a two-step, induced-fit model accounts for the inhibition kinetics (Figure 2).¹⁴ The slow step is characterized by rate constants k_2 and k_{-2} of 0.46 and 0.041 min⁻¹, respectively, suggesting that isomerization of the inhibitor ternary complex occurs 1,000 to 10,000 times slower than the rate of substrate turnover.

In order to rationally modulate residence time in this system, the structural changes that accompany the slow step in enzyme

Received: December 6, 2013

Accepted: February 14, 2014

Published: February 14, 2014



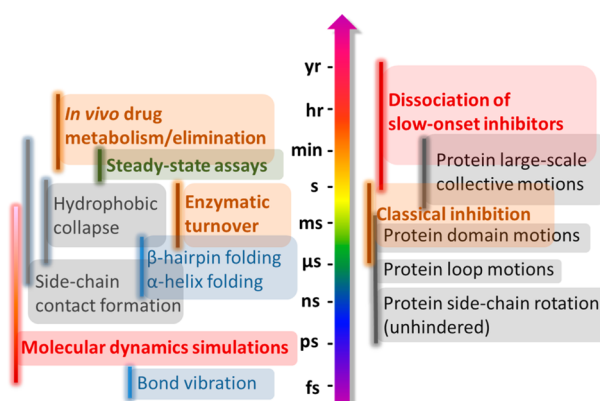


Figure 1. Time scale of slow-onset inhibition. The rates of many common protein motions are shown, ranging from bond vibrations and enzyme turnover to slow-onset inhibition.^{1,28,47–49} Also shown is the time scale for drug pharmacokinetics and the time scales for enzyme assays and MD simulations.^{50–53}

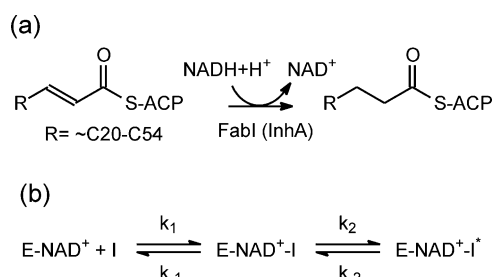


Figure 2. InhA reaction mechanism and induced-fit inhibition. (a) The reaction catalyzed by the FabI enoyl-ACP reductase InhA. (b) The kinetic mechanism for two-step, induced-fit inhibition of InhA by the diphenyl ether inhibitors.

inhibition must be elucidated. In the FabI enzyme class, of which InhA is a member, the kinetics of enzyme inhibition have been linked to structural changes of the substrate binding loop (SBL), a loop of amino acids covering the surface of the substrate binding pocket (residues 197–210 in InhA).^{4,7,8,12,14–17} In the case of the PT70 ternary complex, the SBL forms a helix (helix-6) that closes over the active site and occludes the portal that admits the substrate to the active site.¹⁴ This closed structure contrasts with that observed for the ternary InhA complex in which a substrate analogue (C16-NAC) is bound to the enzyme and in which helix-6 maintains a topology such that the substrate portal remains open.¹⁸ The open conformation is also observed in other catalytically relevant complexes such as the binary InhA:NADH complex (Supplementary Figure S1).¹⁹

In the present work we demonstrate that the open SBL conformation is also found in the structure of the 4-pyridone inhibitor PT155 (Table 1) bound to InhA. Significantly, PT155, despite its structural similarity to PT70, does not exhibit slow-onset inhibition kinetics, suggesting that the open and closed conformations of helix-6 may distinguish the enzyme structure in the EI and EI* complexes on the PT70 binding coordinate. These structures have subsequently been used as the limits for molecular dynamics simulations that map the structural change leading from open to closed conformations of helix-6. On the basis of this analysis, we propose a diphenyl ether binding model in agreement with kinetic, crystallographic, and simulation data in which InhA can be

transformed into a structural state incapable of natural substrate turnover in a slow process kinetically and energetically separated from catalysis. Not only does this provide a foundation for the rational modulation of residence time in this system, the studies also represent one of the few examples of slow-onset inhibition in which a structural basis for the slow step has been elucidated. Although slow-onset inhibition kinetics has been observed in many enzyme systems, description of the accompanying structural change is often elusive due to the transient nature of the initial EI complex,²⁰ and the number of systems where this process has been studied in detail is relatively small.^{21–24} As we demonstrate here, computational methods are invaluable for bridging the gap between kinetic and structural studies of protein motion.

RESULTS AND DISCUSSION

Slow-Onset Inhibition and the Substrate Binding Loop.

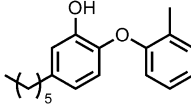
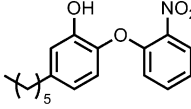
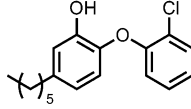
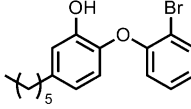
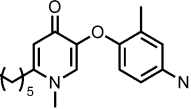
Previously we reported the synthesis and characterization of a series of diphenyl ether InhA inhibitors that differed in the length of the alkyl chain attached to the inhibitor A ring (Table 1).⁸ The affinity of these inhibitors for InhA increased up to an alkyl chain length of 8 carbons, and the most potent compound had a K_i value of 1 nM. X-ray structures of complexes formed by two of these compounds, PT03 (PDB code 2B36) and PT05 (PDB code 2B37), displayed disordered substrate binding loops, consistent with the belief at that time that this loop was ordered only in the presence of slow-onset inhibitors.⁸ In support of this model, when we subsequently designed the slow-onset InhA inhibitor PT70, we observed an ordered substrate-binding loop in the structure of the corresponding ternary complex (PDB code 2X22 and 2X23).¹⁴

Opening of Substrate Binding Loop in a Complex Formed with a Rapid-Reversible Inhibitor.

A breakthrough in our understanding of the structural changes that accompany slow-onset inhibition was revealed by the X-ray structure of the rapid-reversible 4-pyridone inhibitor PT155 bound to InhA (Figure 3, Table 1). Superposition of the PT155 and PT70 ternary complex structures reveals that the 4-pyridone inhibitor occupies the same space in the active site as that observed for the diphenyl ether compounds. In addition, unlike the structure of PT03 bound to InhA, clear density can be observed for the substrate binding loop in the PT155 structure (Supplementary Figures S2 and S3). However, in contrast to the PT70 structure, helix-6 has moved away from strand-4 in the PT155 structure and instead occupies a position that is very similar to that of the substrate binding loop in the X-ray structure determined by Sacchettini and co-workers of the complex formed between InhA, NAD⁺, and the C16 fatty acid substrate analogue C16NAC (PDB code 1BVR).¹⁸ In both the C16NAC and PT155 ternary complexes, helix-6 adopts a conformation (open conformation) that is about 10 Å from strand-4 on the opposite side of the substrate-binding crevice, whereas in the PT70 ternary complex helix-6 establishes extensive interactions with PT70 and makes van der Waals contacts with strand-4 (closed conformation) (Figure 3).

Open and Closed Conformations: Catalysis and Enzyme ‘Self’ Inhibition. In order to substantiate the relationship between slow-onset inhibition and the position of helix-6, we determined the structures of three additional slow-onset diphenyl ether inhibitors bound to InhA: PT10, PT91, and PT92 (Table 1, Supplementary Table S1 and S2). In each case ternary complexes formed by these inhibitors adopt the closed conformation. In contrast, similar to the C16-

Table 1. Structural and Kinetic Data for InhA Inhibitors

Compound	K_i or K_i^* (nM) ^a	k_{off} (min ⁻¹)	Loop ^e	
	PT70 ^a	0.022 ± 0.001	0.043 ± 0.006	Closed
	PT10 ^b	129 ± 77	0.037 ± 0.022	Closed
	PT91 ^b	0.96 ± 0.14	0.048 ± 0.007	Closed
	PT92 ^b	0.20 ± 0.05	0.033 ± 0.011	Closed
	PT155 ^c	40 ± 12	RR ^d	Open

^aFrom Luckner et al.¹⁴ ^b K_i^* and k_{off} values were determined by progress curve analysis. ^c K_i determined by steady state kinetics. ^dRR, rapid reversible, no evidence of slow-onset inhibition. ^eDominant substrate-binding loop (SBL) conformation.

NAC and PT155 structures, the open conformation of helix-6 is observed in the structures of apo and binary InhA complexes (Supplementary Figure S1). The open conformation of helix-6 is catalytically relevant since the opening (portal) between helix-6 and strand-4 provides the space proposed for ACP to dock with InhA and deliver the long fatty acyl substrate (C24–C50) into the active site.¹⁸ However, the substrate portal is blocked by helix-6 when PT70 is bound (Supplementary Figure S4). In Figure 4a it can be seen that the relative orientation of helix-6 with respect to helix-7 remains similar to the binary complex (PDB code 2AQ8) when the substrate ternary complex is formed. In contrast, binding with PT70 results in a different relative orientation after significant rotation, translation as well as an internal twist of helix-6. This conformational change brings about shuffling of the helix-6 residues such that their functional roles are altered. For example, the solvent-exposed V203, used primarily to maintain the structural integrity in either the binary complex or the substrate ternary complex, is involved in ligand binding in the PT70 ternary complex.

In the ternary complex of the rapid-reversible analogue PT155, the portal-open conformation becomes dominant (Figure 3c, Supplementary Figures S2 and S3). In addition to the presence of PT155 in the active site, ordered buffer components are observed wrapping around the substrate portal and thus revealing the potential binding sites for the long aliphatic tail and phosphopantetheine arm of the natural substrate (Supplementary Figure SSa). When the closed structure is superimposed onto the PT155 bound structure, it can be seen that helix-6 partially mimics the natural substrate, engaging recognition elements of InhA (Supplementary Figure SSb). Specifically, A201, I202, and V203 on helix-6 mimic part

of the fatty acid tail, while L197 mimics part of the phosphopantetheine group. Thus, the potency of PT70 arises not only from its competition with the thioester moiety and the initial portion of the fatty acyl chain of the substrate but also from its effect on the conformation of helix-6, which competes with the rear portion of the fatty acyl chain as well as the phosphopantetheine arm. In other words, helix-6 itself becomes an inhibitor, and binding of PT70 has an impact beyond the protein–inhibitor interface.²⁵ This is a fascinating example of how a small inhibitor may reproduce the structure of a much larger substrate by taking advantage of enzyme flexibility.

Transition between Open and Closed Conformations.

Taken together, crystal structures of the slow-onset and rapid-reversible ternary complexes suggest that there exist two major enzyme conformations from which the diphenyl ether may select, thus influencing the binding kinetics. Since slow inhibition lags about 4 orders of magnitude behind the rate of catalysis (Figure 4b, Table 1),^{26,27} structural conversions between these two major enzyme conformers when bound to inhibitor must be separated by a much larger energy barrier than that between any conformers on the catalytic reaction coordinate. In addition, since helix-6 occupies portions of the active site in the closed conformation that would normally bind substrate, we also propose that the conformation observed in EI* lies off the catalytic pathway. This also suggests that the portal-open conformer might represent the EI complex in the two-step, induced-fit inhibitor binding mechanism (Figure 2). This hypothesis is illustrated in the one-dimensional energy profiles of the enzyme in the presence and absence of the inhibitor (Figure 4c) where the hierarchical time scales of inhibition and catalysis are shown schematically.²⁸ This structural understanding provides a framework to examine

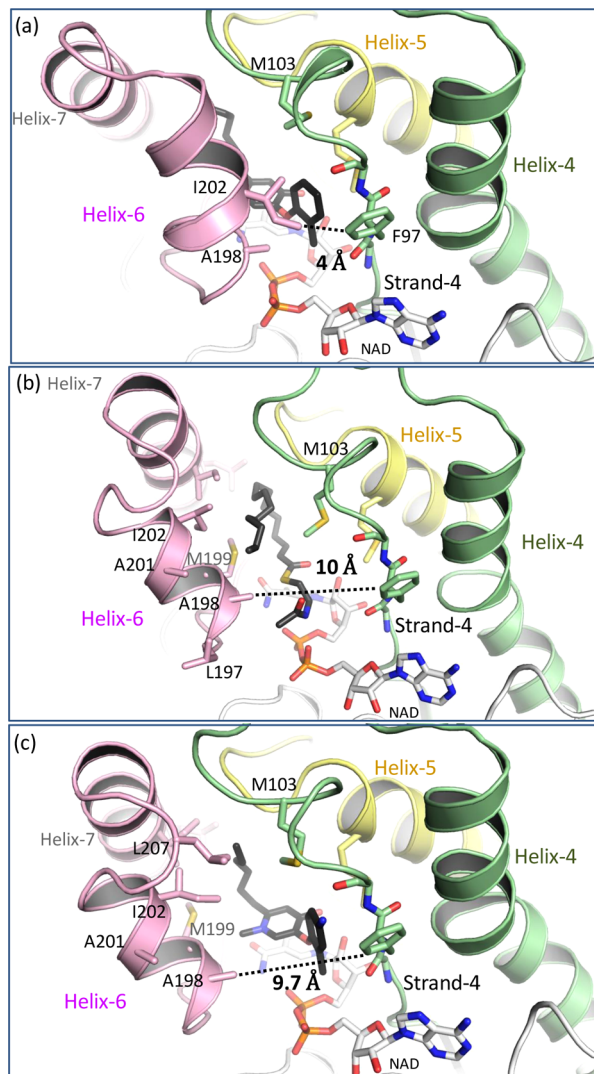


Figure 3. Open and closed conformations of InhA. (a) Structure of the closed state is represented by the PT70 ternary complex (PDB code 2X23, chain A)¹⁴ in which helix-6 is close to strand-4. (b) Structure of the open state is represented by the C16-NAC ternary complex (PDB code 1BVR, chain A)¹⁸ in which helix-6 has moved away from strand-4 to accommodate the substrate. (c) Structure of the PT155 ternary complex observed in chain B in the I₂12₁ crystal.

energetic changes along the induced-fit reaction coordinate in Figure 2.^{29,30}

Simulation of the Isomerization Path and the Free Energy Profile. We propose that the open conformation adopted in the substrate-bound and PT155 ternary complexes is equivalent to the structure of the *initial* EI complex formed when PT70 binds to InhA and that the slow step in formation of the final EI* complex involves movement of helix-6 and -7 relative to each other. To determine the structure and corresponding energetics of the open to closed conformational change, a suitable computational method is needed. Since the time scale of the open to closed isomerization process is beyond the limit of current time-dependent MD simulations, a series of intermediate conformations were generated using the time-independent partial nudged elastic band (PNEB) method.³¹ In this approach, a series of simulations are coupled together and run simultaneously, like beads on a string, mapping the multidimensional low-energy path connecting the

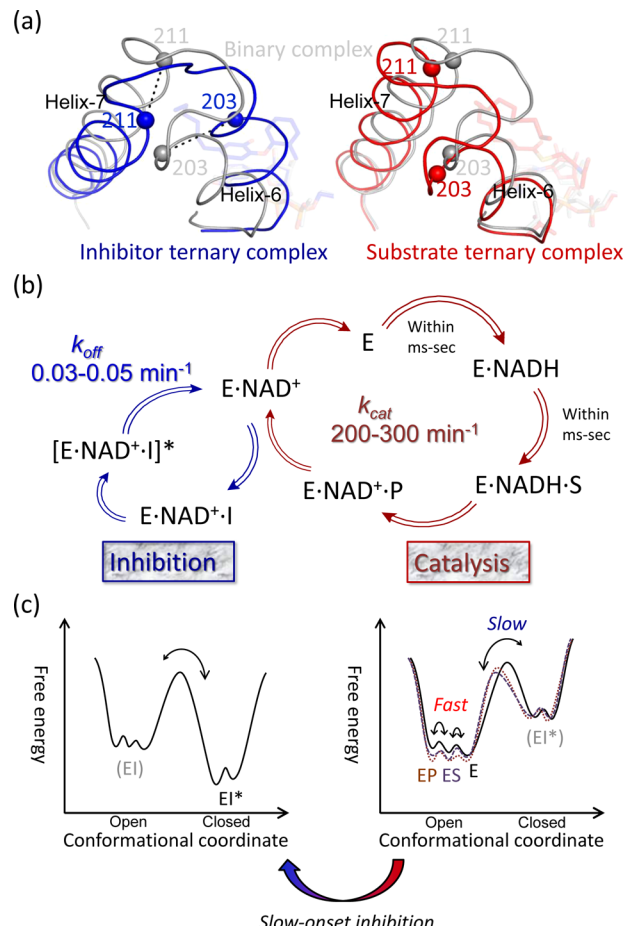


Figure 4. Kinetics, structural and energetic changes in InhA inhibition and catalysis. (a) Comparison of the conformational changes resulting from slow inhibition and substrate binding. Helix-6/helix-7 from the cofactor-bound binary complex is shown in gray in both overlays. PT70 (PDB code 2X23, chain B) and substrate analogue (PDB code 1BVR, chain A) ternary complexes are shown in blue on the left and in red on the right, respectively. Ca of residue 203 and 211 are highlighted, showing relative motions of helix-6 with respect to helix-7. (b) Difference in the kinetic rates involved in the inhibition and the catalytic cycle. The slow rates in the inhibition cycle relative to those in the catalytic cycle result in time-dependent inhibition observed in the InhA kinetic assay. The inhibition cycle is shown for diphenyl ethers, which form a ternary complex with the cofactor through the two-step, induced-fit mechanism. In the absence of the inhibitor, the equilibrium with the Michaelis complex, E·NADH-S, is reached rapidly on the time scale of the enzyme assay. (c) Proposed 1D energy profiles before (right) and after (left) binding of a slow inhibitor (solid line). The right and left energy landscapes depict the initial and final cross sections on the binding reaction coordinate for slow-onset inhibition as shown in Figure 2. Black solid line, violet dashed line, and brown dotted lines in the right panel depict the change in landscape that occurs during catalysis. E, ES, and EP denote the cofactor binary complex, substrate ternary complex, and product ternary complex, respectively; EI and EI* denote the inhibitor ternary complexes in Figure 2.

two end point (crystal) structures. Each of the all-atom “bead” simulations undergoes normal dynamics, with the exception that neighboring simulations have forces modified to keep them spaced at intervals between the end points. Two-dimensional free energy profiles along the NEB-optimized pathway were then obtained by umbrella sampling along two torsion angles (step and shear) that were chosen to describe the relative

motions of helix-6 and helix-7 (Figure 5). By this definition, the open structures, such as the cofactor-bound binary complex and

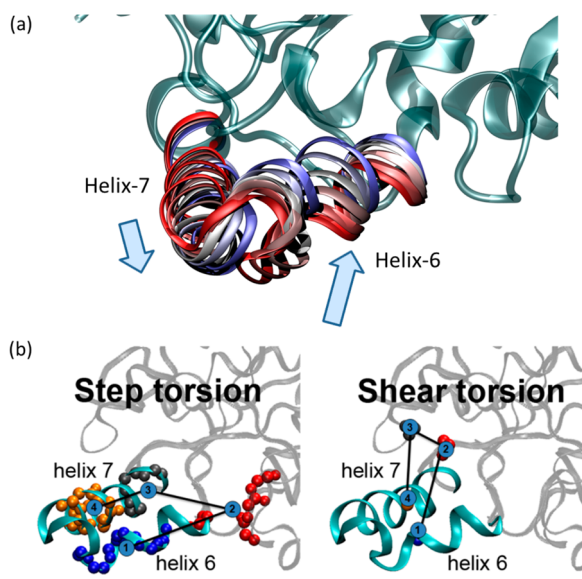


Figure 5. Open to closed transition determined by the computational approach. (a) The colors (red to blue) represent structures along the reaction coordinate. Helix6 has larger scale of motion compared to helix7. (b) Definition of step and shear torsions that reduce the dimensionality of the structural change.

the substrate analogue-bound ternary complex, are found in the range of step torsion angles between 5° to 20° and shear torsion angles between -5° to 5° , while the closed structures, such as the PT70 ternary complex, is found at step and shear torsion angles between -30° to -10° and -15° to 7° , respectively.

Energetic Basis of Slow-Onset Inhibition. The free energy profiles that result from the computational analysis are shown in Figure 6 where it can be seen that there is good agreement with the observed structural and kinetic data for enzyme inhibition: The open conformation of helix-6 is more stable for both the cofactor-bound binary complex and the PT155 ternary complex, while the closed form is more stable when PT70 is bound to the enzyme. This analysis was repeated for the PT70 analogue PT92 (Table 1), which is also a slow-onset inhibitor and is also found to stabilize the closed state of the enzyme. The energy scales reveal that binding of PT70 or PT92 to the binary complex will encounter an energy barrier of at least 4–6 kcal/mol to convert the open enzyme to the closed one. The activation energy for dissociation of PT70 is estimated to be on the order of 10 kcal/mol (data not shown), and the energy profiles of the binary and PT70 ternary complexes qualitatively reproduce this barrier. Umbrella sampling requires a small number of well-defined reaction coordinate(s), which can be challenging to define for a process where a large number of amino acids change conformation; thus the computational results serve as a qualitative guide to interpreting the experimental measurements.

The energy profile analysis also allows us to rationalize data for PT03 for which a disordered substrate binding loop has previously been reported. In Figure 6 it can be seen that while the closed state of the InhA:NAD⁺:PT03 ternary complex is more stable than the open state, the energy difference between the two states is less than 1 kcal/mol with a small barrier of 3–

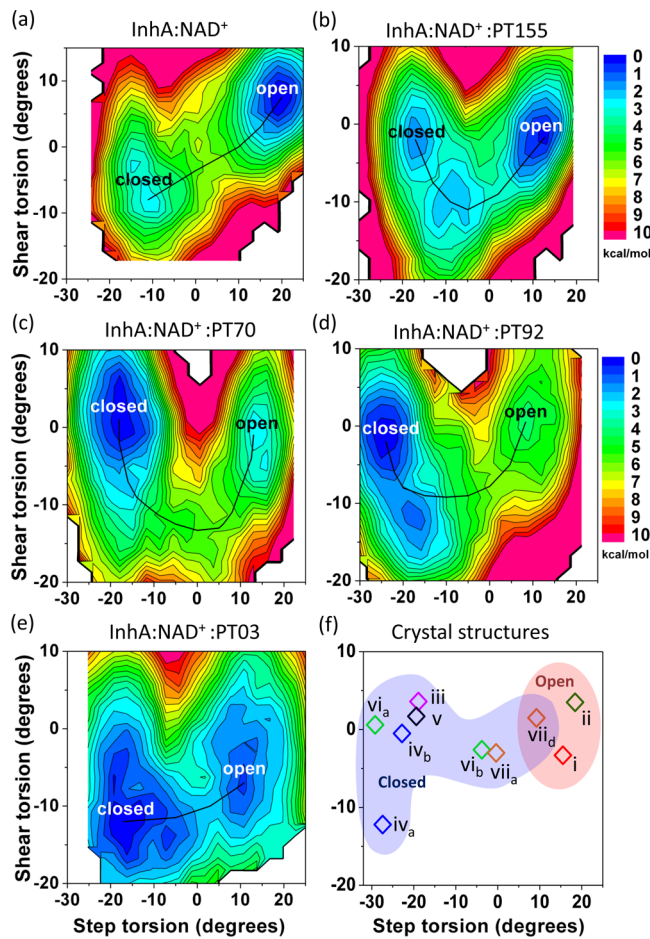


Figure 6. Free energy profiles and summary of X-ray structural data. Free energy profiles are shown for (a) the cofactor-bound binary complex, (b) the PT155 ternary complex, (c) the PT70 ternary complex, (d) the PT92 ternary complex, and (e) the PT03 ternary complex. (f) Locations of crystal structures on the same conformational coordinates. Area occupied by open structures is shaded red; area occupied by diphenyl ether ternary complex structures is shaded blue: (i) E-NADH binary complex 2AQ8; (ii) C16-NAC ternary complex 1BVR; (iii) PT70 ternary complex 2X23, chain A; (iv_a) PT10 ternary complex, chain A; (iv_b) PT10 ternary complex, chain B; (v) PT91 ternary complex; (vi_a) PT92 ternary complex, chain A; (vi_b) PT92 ternary complex, chain B; (vii_a) PT155 ternary complex, chain A, P2₁2₁2₁ crystal; (vii_d) PT155 ternary complex, chain D, P2₁2₁ crystal.

4 kT at RT, thus predicting that interconversion between the two states will occur within microseconds.²⁸ Interestingly, although it is difficult to interpret the density for the substrate binding loop, residual density can be found for both the open and closed positions of helix-6 in two subunits of the crystal structure (Supplementary Figure S6), indicating that both states are partially populated in the X-ray structure. Thus when bound to PT03 in the crystal, helix-6 is likely in a state of dynamic disorder which occasionally turns to static disorder³² as a result of crystal packing effects. This observation is consistent with our original interpretation that the substrate-binding loop for this complex is disordered and is also in line with the free energy profile calculated for this inhibitor. The kinetic, structural, and energetic data together suggest that ortho substitution on the inhibitor B ring and the extra tail length on the A ring can stabilize the EI* state while the

transition state on the binding coordinate is destabilized, resulting in an increased barrier for inhibitor dissociation.

Intermediate Structures on the Reaction Coordinate from X-ray Crystallographic Analysis. The observation of residual density for both open and closed states in the InhA:NAD⁺:PT03 ternary complex structure prompted us to obtain additional structures of InhA inhibitor complexes, and we also solved the structures of the slow-onset inhibitors PT10 and PT92 bound to InhA (Table 1). Both PT10 and PT92 have similar residence times for InhA compared to PT70 and PT91. However, while the ternary complex structures of PT70 and PT91 give only a single, closed conformation, monomers in the asymmetric units of the PT10 and PT92 ternary complexes exist in two conformations that populate different areas on the shear-step torsion landscape (Figure 6f). While the two conformations observed for the PT10 ternary complex have step torsion angles in the closed region of the plot, one of the monomers in the PT92 structure has a step torsion angle intermediate between open and closed. Similarly, further analysis of the PT155 ternary complex structures reveals that some of these monomers also have step torsion angles intermediate between the open and closed states. Although the intermediate structures observed for PT92 and PT155 are in the high energy regions of the two-dimensional free energy profiles, we believe that these structures are stabilized by crystal contacts, a proposal that is supported by the observation that intermediate structures are found only in some monomers.^{33,34} Thus, taken together, the existing structural and thermodynamic data map the conformational transition from the open to closed states.

Slow Isomerization Is a Large-Scale Refolding Process. The energy profiles in Figure 6 show that the enzyme has to overcome a major energy barrier around step torsion zero to convert between the open and closed states. As noted above high-energy structures in this conformation are observed in the asymmetric unit of the PT92 and PT155 ternary complexes (Figure 6f). The structural data reveal a variety of binding modes in which hydrophobic residues on helix-6 and helix-7, including M199, I202, V203, L207, and I215, explore different modes of interaction with the inhibitor as well as with other structural elements from the enzyme itself. This provides a dynamic picture of how barrier-crossing is accompanied by large-scale refolding of the ternary complex that directly or indirectly impacts the packing modes of at least 30 residues and at the subunit interfaces (Figure 7, Supplementary Figures S7, S8, and S9). The macroscopic two-step, induced-fit process upon slow inhibition is thus a consequence of many microscopic refolding steps driven by the interactions with the diphenyl ether.

Current Understanding of EI to EI* Isomerization. Conversion of EI to EI* on the reaction coordinate for inhibition of InhA requires a large amplitude conformational change. While such large-scale structural changes have not been identified in most cases of slow-onset inhibition, it is likely that stabilization of a rarely sampled structural state needs to occur, as demonstrated by our energy profiles.^{35,36} In the case of InhA, stabilization is caused by the diphenyl ether inhibitors, which are thought to be bound to the enzyme in their deprotonated forms and are thus transition state analogues of the enzyme catalyzed reaction.^{7,12} It is believed that transition state analogues that bind through an induced-fit mechanism do so by transforming a dynamic transient state into a thermodynamically stable state,³⁷ and systems where this phenomenon has

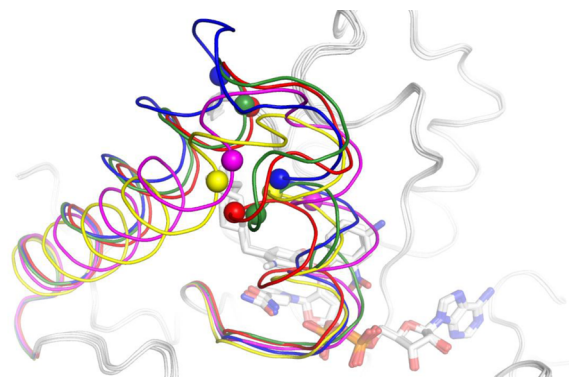


Figure 7. Helix-6 and -7 conformations along the open to closed reaction coordinate. Structures are taken from the binary complex (PDB code 2AQ8, red), PT155 ternary complex (P2₁2₁ chain C/D, green), PT92 ternary complex (blue), PT10 ternary complex (yellow), and PT70 ternary complex (purple). Individual structures are shown in Supplementary Figure S7.

been studied in detail include the transition state analogue inhibitors of purine nucleoside phosphorylases such as 5'-methylthioadenosine phosphorylase.²¹ While conformational states stabilized by transition state analogues might potentially also be present during normal substrate turnover, the diphenyl ether inhibitors mimic only a portion of the transition state formed during substrate reduction. In the closed conformation helix-6 occupies portions of the active site where the enoyl-ACP substrate is expected to bind, and thus it is likely that the enzyme conformation observed in EI* is not on the reaction pathway for the normal catalytic cycle of InhA. Further microscopic investigation of the slow isomerization process may lead to a better understanding of enzyme inhibition where large-amplitude conformational changes have not been identified.

Conclusion. Using a combination of enzyme kinetics, structural biology, and molecular dynamics simulations, we have identified a large-scale conformational change that accounts for the slow conversion of EI to EI* in the two-step, induced-fit inhibition of InhA by the diphenyl ether class of compounds. Analogs of the slow-onset inhibitor PT70 were used to identify the structure of the initial EI complex, which was found to be very similar to the structure of the enzyme–substrate complex. Energy profiles were then calculated using the structures of EI and EI* as the initial and final points on the reaction coordinate leading from the open to the closed state. The energy profiles rationalize the observed kinetics for inhibition of the enzyme by rapid reversible and slow-onset inhibitors and provide a framework for the rational modulation of residence time in this enzyme system. Our findings suggest that the structural basis for slow-onset kinetics can be understood once the structures of both EI and EI* have been identified, thus providing a framework for undertaking the rational control of enzyme–inhibitor binding kinetics.

METHODS

Protein Purification and Enzyme Kinetics. Wild-type InhA was expressed and purified as described previously.^{14,38} PT10, PT91, and PT92 were available from previous studies.^{13,39} The synthesis of PT155 and the kinetics for the interaction of the compounds with InhA are being published elsewhere.

Crystallization and Structure Determination of the InhA Ternary Complexes with PT92, PT10, PT91, and PT155. X-ray

structures of the ternary complexes formed between InhA, NAD⁺ and each inhibitor were determined as described in the supplementary methods. Diffraction data were collected at beamlines X29, X2S, and X12C at NSLS. The image frames were indexed, integrated, and scaled using HKL2000,⁴⁰ and structures were solved using MolRep.⁴¹ Structure refinement was performed in Phenix.⁴² Data collection and refinement statistics are given in Supplementary Table S1.

Computational Methods. The conformational change pathway and associated free energy profile for the transition from the open (E1) to closed (E1*) conformations was generated following our previous work,⁴³ using the partial nudged elastic band (PNEB)³² variant of the nudged elastic band simulation approach⁴⁴ followed by umbrella sampling as described in Supplementary Methods. The initial closed and open structures were taken from the first monomers of the InhA:NAD⁺:PT70 complex (PDB code 2X23¹⁴) and the InhA:NAD⁺:C16-NAC complex (PDB code 1BVR¹⁸), respectively, while DOCK 6.3⁴⁵ was used to generate the initial poses for the other inhibitors. The equilibrated open and closed structures were assigned as the two end-point structures, and 30 windows (including endpoints) were used in PNEB. Simulated annealing was used to optimize the local energy-minimized path. Subsequently, energy landscape plots were obtained using umbrella sampling in which two reaction coordinates (step and shear torsions) were used to describe the motion of α -helices 6 and 7 (Figure 5). The weighted histogram analysis (WHAM)⁴⁶ approach was then used to generate the potential of mean force (PMF) from the umbrella sampling results.

■ ASSOCIATED CONTENT

Supporting Information

Supplemental methods and tables of data collection and refinement statistics for the X-ray crystallographic studies, additional analysis of the PT155 and PT03 ternary complex structures, additional analysis of the open to closed transition, and partial charges of compounds. This material is available free of charge via the Internet at <http://pubs.acs.org>.

Accession Codes

Atomic coordinates have been deposited in the Protein Data Bank (PDB) with the accession codes 4OHU, 4OXK, 4OXN, 4OXY, and 4OYR.

■ AUTHOR INFORMATION

Corresponding Authors

*E-mail: carlos.simmerling@stonybrook.edu.
*E-mail: peter.tonge@stonybrook.edu.

Author Contributions

#These authors contributed equally to this work.

Notes

The authors declare no competing financial interest.

■ ACKNOWLEDGMENTS

This work was supported by GM102864 from the National Institutes of Health (NIH) to P.J.T. X-ray data were measured at NSLS, financial support for which comes principally from the DOE and from NCRR NIH Grant P41RR012408. This research utilized resources at the New York Center for Computational Sciences supported by DOE under Contract No. DE-AC02-98CH10886 and by the State of New York. This research was also supported in part by NSF through TeraGrid resources provided by NICS under grant number TG-CHE100107 and TG-MCA02N028 to C.S.

■ REFERENCES

- (1) Schloss, J. V. (1988) Significance of slow-binding enzyme-inhibition and its relationship to reaction-intermediate analogs. *Acc. Chem. Res.* 21, 348–353.

(2) Morrison, J. F., and Walsh, C. T. (1988) The behavior and significance of slow-binding enzyme inhibitors. *Adv. Enzymol. Relat. Areas Mol. Biol.* 61, 201–301.

(3) Copeland, R. A., Pompliano, D. L., and Meek, T. D. (2006) Drug-target residence time and its implications for lead optimization. *Nat. Rev. Drug Discovery* 5, 730–739.

(4) Lu, H., England, K., am Ende, C., Truglio, J. J., Luckner, S., Reddy, B. G., Marlenee, N. L., Knudson, S. E., Knudson, D. L., Bowen, R. A., Kisker, C., Slayden, R. A., and Tonge, P. J. (2009) Slow-onset inhibition of the FabI enoyl reductase from *Francisella tularensis*: residence time and in vivo activity. *ACS Chem. Biol.* 4, 221–231.

(5) Copeland, R. A. (2011) Conformational adaptation in drug-target interactions and residence time. *Future Med. Chem.* 3, 1491–1501.

(6) Swinney, D. C. (2009) The role of binding kinetics in therapeutically useful drug action. *Curr. Opin. Drug Discovery Dev.* 12, 31–39.

(7) Chang, A., Schiebel, J., Yu, W., Bommineni, G. R., Pan, P., Baxter, M. V., Khanna, A., Sottriffer, C. A., Kisker, C., and Tonge, P. J. (2013) Rational optimization of drug-target residence time: insights from inhibitor binding to the *Staphylococcus aureus* FabI enzyme-product complex. *Biochemistry* 52, 4217–4228.

(8) Sullivan, T. J., Truglio, J. J., Boyne, M. E., Novichenok, P., Zhang, X., Stratton, C. F., Li, H.-J., Kaur, T., Amin, A., Johnson, F., Slayden, R. A., Kisker, C., and Tonge, P. J. (2006) High affinity InhA inhibitors with activity against drug resistant strains of *Mycobacterium Tuberculosis*. *ACS Chem. Biol.* 1, 43–53.

(9) Rafi, S. B., Cui, G., Song, K., Cheng, X., Tonge, P. J., and Simmerling, C. (2006) Insight through molecular mechanics Poisson-Boltzmann surface area calculations into the binding affinity of triclosan and three analogues for FabI, the *E. coli* enoyl reductase. *J. Med. Chem.* 49, 4574–4580.

(10) Lu, H., and Tonge, P. J. (2008) Inhibitors of FabI, an enzyme drug target in the bacterial fatty acid biosynthesis pathway. *Acc. Chem. Res.* 41, 11–20.

(11) Pan, P., and Tonge, P. J. (2012) Targeting InhA, the FASII enoyl-ACP reductase: SAR studies on novel inhibitor scaffolds. *Curr. Top. Med. Chem.* 12, 672–693.

(12) Schiebel, J., Chang, A., Lu, H., Baxter, M. V., Tonge, P. J., and Kisker, C. (2012) *Staphylococcus aureus* FabI: inhibition, substrate recognition, and potential implications for in vivo essentiality. *Structure* 20, 802–813.

(13) Pan, P., Knudson, S., Bommineni, G. R., Li, H. J., Lai, C. T., Liu, N., Yu, W., Garcia-Diaz, M., Simmerling, C., Patil, S. S., Slayden, R. A., Tonge, P. J. (2014) Time-dependent diaryl ether inhibitors of InhA, the *M. tuberculosis* enoyl-ACP reductase: SAR studies of enzyme inhibition and in vivo antibacterial activity. *ChemMedChem*, in press.

(14) Luckner, S. R., Liu, N., Am Ende, C. W., Tonge, P. J., and Kisker, C. (2010) A slow, tight-binding inhibitor of InhA, the enoyl-ACP reductase from *Mycobacterium tuberculosis*. *J. Biol. Chem.* 285, 14330–14337.

(15) Levy, C. W., Roujeinikova, A., Sedelnikova, S., Baker, P. J., Stuitje, A. R., Slabas, A. R., Rice, D. W., and Rafferty, J. B. (1999) Molecular basis of triclosan activity. *Nature* 398, 383–384.

(16) da Costa, A. L., Pauli, I., Dorn, M., Schroeder, E. K., Zhan, C. G., and de Souza, O. N. (2012) Conformational changes in 2-trans-enoyl-ACP (CoA) reductase (InhA) from *M. tuberculosis* induced by an inorganic complex: a molecular dynamics simulation study. *J. Mol. Model.* 18, 1779–1790.

(17) Hevener, K. E., Mehboob, S., Su, P. C., Truong, K., Boci, T., Deng, J., Ghassemi, M., Cook, J. L., and Johnson, M. E. (2012) Discovery of a novel and potent class of *F. tularensis* enoyl-reductase (FabI) inhibitors by molecular shape and electrostatic matching. *J. Med. Chem.* 55, 268–279.

(18) Rozwarski, D. A., Vilchez, C., Sugantino, M., Bittman, R., and Sacchettini, J. C. (1999) Crystal structure of the *Mycobacterium tuberculosis* enoyl-ACP reductase, InhA, in complex with NAD⁺ and a C16 fatty acyl substrate. *J. Biol. Chem.* 274, 15582–15589.

(19) Oliveira, J. S., Pereira, J. H., Canduri, F., Rodrigues, N. C., de Souza, O. N., de Azevedo, W. F., Jr., Bassi, L. A., and Santos, D. S.

- (2006) Crystallographic and pre-steady-state kinetics studies on binding of NADH to wild-type and isoniazid-resistant enoyl-ACP(CoA) reductase enzymes from *Mycobacterium tuberculosis*. *J. Mol. Biol.* 359, 646–666.
- (20) Garvey, E. P. (2010) Structural mechanisms of slow-onset, two-step enzyme inhibition. *Curr. Chem. Biol.* 4, 64–73.
- (21) Guan, R., Ho, M. C., Brenowitz, M., Tyler, P. C., Evans, G. B., Almo, S. C., and Schramm, V. L. (2011) Entropy-driven binding of picomolar transition state analogue inhibitors to human 5'-methylthioadenosine phosphorylase. *Biochemistry* 50, 10408–10417.
- (22) Fieulaine, S., Boulairet, A., Artaud, I., Desmadril, M., Dardel, F., Meinnel, T., and Giglione, C. (2011) Trapping conformational states along ligand-binding dynamics of peptide deformylase: the impact of induced fit on enzyme catalysis. *PLoS Biol.* 9, e1001066.
- (23) Carroll, M. J., Mauldin, R. V., Gromova, A. V., Singleton, S. F., Collins, E. J., and Lee, A. L. (2012) Evidence for dynamics in proteins as a mechanism for ligand dissociation. *Nat. Chem. Biol.* 8, 246–252.
- (24) Pan, A. C., Borhani, D. W., Dror, R. O., and Shaw, D. E. (2013) Molecular determinants of drug-receptor binding kinetics. *Drug Discovery Today* 18, 667–673.
- (25) Teague, S. J. (2003) Implications of protein flexibility for drug discovery. *Nat. Rev. Drug Discovery* 2, 527–541.
- (26) Parikh, S., Moynihan, D. P., Xiao, G. P., and Tonge, P. J. (1999) Roles of tyrosine 158 and lysine 165 in the catalytic mechanism of InhA, the enoyl-ACP reductase from *Mycobacterium tuberculosis*. *Biochemistry* 38, 13623–13634.
- (27) Quemard, A., Sacchettini, J. C., Dessen, A., Vilchez, C., Bittman, R., Jacobs, W. R., Jr., and Blanchard, J. S. (1995) Enzymatic characterization of the target for isoniazid in *Mycobacterium tuberculosis*. *Biochemistry* 34, 8235–8241.
- (28) Henzler-Wildman, K., and Kern, D. (2007) Dynamic personalities of proteins. *Nature* 450, 964–972.
- (29) Rawat, R., Whitty, A., and Tonge, P. J. (2003) The isoniazid-NAD adduct is a slow, tight-binding inhibitor of InhA, the *Mycobacterium tuberculosis* enoyl reductase: Adduct affinity and drug resistance. *Proc. Natl. Acad. Sci. U.S.A.* 100, 13881–13886.
- (30) Hammes-Schiffer, S. (2013) Catalytic efficiency of enzymes: a theoretical analysis. *Biochemistry* 52, 2012–2020.
- (31) Bergonzo, C., Campbell, A. J., Walker, R. C., and Simmerling, C. (2009) A partial nudged elastic band implementation for use with large or explicitly solvated systems. *Int. J. Quantum Chem.* 109, 3781–3790.
- (32) Petsko, G. A., and Ringe, D. (1984) Fluctuations in protein structure from X-ray diffraction. *Annu. Rev. Biophys. Bioeng.* 13, 331–371.
- (33) Vonrhein, C., Schlauderer, G. J., and Schulz, G. E. (1995) Movie of the structural changes during a catalytic cycle of nucleoside monophosphate kinases. *Structure* 3, 483–490.
- (34) Beckstein, O., Denning, E. J., Perilla, J. R., and Woolf, T. B. (2009) Zipping and unzipping of adenylate kinase: atomistic insights into the ensemble of open<→>closed transitions. *J. Mol. Biol.* 394, 160–176.
- (35) Frieden, C. (1979) Slow transitions and hysteretic behavior in enzymes. *Annu. Rev. Biochem.* 48, 471–489.
- (36) Casey, A. K., Baugh, J., and Frantom, P. A. (2012) The slow-onset nature of allosteric inhibition in alpha-isopropylmalate synthase from *Mycobacterium tuberculosis* is mediated by a flexible loop. *Biochemistry* 51, 4773–4775.
- (37) Schramm, V. L. (2013) Transition states, analogues, and drug development. *ACS Chem. Biol.* 8, 71–81.
- (38) Parikh, S. L., Xiao, G., and Tonge, P. J. (2000) Inhibition of InhA, the enoyl-reductase from *Mycobacterium tuberculosis*, by triclosan and isoniazid. *Biochemistry* 39, 7645–7650.
- (39) am Ende, C. W., Knudson, S. E., Liu, N., Childs, J., Sullivan, T. J., Boyne, M., Xu, H., Gegina, Y., Knudson, D. L., Johnson, F., Peloquin, C. A., Slayden, R. A., and Tonge, P. J. (2008) Synthesis and in vitro antimycobacterial activity of B-ring modified diaryl ether InhA inhibitors. *Bioorg. Med. Chem. Lett.* 18, 3029–3033.
- (40) Otwinowski, Z., and Minor, W. (1997) Processing of X-ray diffraction data collected in oscillation mode. *Methods Enzymol.* 276, 307–326.
- (41) Vagin, A., and Teplyakov, A. (1997) MOLREP: an automated program for molecular replacement. *J. Appl. Crystallogr.* 30, 1022–1025.
- (42) Adams, P. D., Afonine, P. V., Bunkoczi, G., Chen, V. B., Davis, I. W., Echols, N., Headd, J. J., Hung, L. W., Kapral, G. J., Grosjean-Kunstleve, R. W., McCoy, A. J., Moriarty, N. W., Oeffner, R., Read, R. J., Richardson, D. C., Richardson, J. S., Terwilliger, T. C., and Zwart, P. H. (2010) PHENIX: a comprehensive Python-based system for macromolecular structure solution. *Acta Crystallogr., Sect. D: Biol. Crystallogr.* 66, 213–221.
- (43) Bergonzo, C., Campbell, A. J., de Los Santos, C., Grollman, A. P., and Simmerling, C. (2011) Energetic preference of 8-oxoG eversion pathways in a DNA glycosylase. *J. Am. Chem. Soc.* 133, 14504–14506.
- (44) Mathews, D. H., and Case, D. A. (2006) Nudged elastic band calculation of minimal energy paths for the conformational change of a GG non-canonical pair. *J. Mol. Biol.* 357, 1683–1693.
- (45) Lang, P. T., Brozell, S. R., Mukherjee, S., Pettersen, E. F., Meng, E. C., Thomas, V., Rizzo, R. C., Case, D. A., James, T. L., and Kuntz, I. D. (2009) DOCK 6: combining techniques to model RNA-small molecule complexes. *RNA* 15, 1219–1230.
- (46) Kumar, S., Rosenberg, J. M., Bouzida, D., Swendsen, R. H., and Kollman, P. A. (1992) THE weighted histogram analysis method for free-energy calculations on biomolecules. I. The method. *J. Comput. Chem.* 13, 1011–1021.
- (47) Schramm, V. L. (2011) Enzymatic transition states, transition-state analogs, dynamics, thermodynamics, and lifetimes. *Annu. Rev. Biochem.* 80, 703–732.
- (48) Chergui, M., and Zewail, A. H. (2009) Electron and X-ray methods of ultrafast structural dynamics: Advances and applications. *ChemPhysChem* 10, 28–43.
- (49) Wu, Y., Kondrashkina, E., Kayatekin, C., Matthews, C. R., and Bilsel, O. (2008) Microsecond acquisition of heterogeneous structure in the folding of a TIM barrel protein. *Proc. Natl. Acad. Sci. U.S.A.* 105, 13367–13372.
- (50) Tummino, P. J., and Copeland, R. A. (2008) Residence time of receptor-ligand complexes and its effect on biological function. *Biochemistry* 47, 5481–5492.
- (51) Werner, T., Morris, M. B., Dastmalchi, S., and Church, W. B. (2012) Structural modelling and dynamics of proteins for insights into drug interactions. *Adv. Drug Deliv. Rev.* 64, 323–343.
- (52) Shaw, D. E., Maragakis, P., Lindorff-Larsen, K., Piana, S., Dror, R. O., Eastwood, M. P., Bank, J. A., Jumper, J. M., Salmon, J. K., Shan, Y., and Wriggers, W. (2010) Atomic-level characterization of the structural dynamics of proteins. *Science* 330, 341–346.
- (53) Voelz, V. A., Bowman, G. R., Beauchamp, K., and Pande, V. S. (2010) Molecular simulation of ab initio protein folding for a millisecond folder NTL9(1–39). *J. Am. Chem. Soc.* 132, 1526–1528.